Time-Bin-Modulated Biphotons from Cavity-Enhanced Down-Conversion

Christopher E. Kuklewicz,* Franco N. C. Wong, and Jeffrey H. Shapiro
Research Laboratory of Electronics, Massachusetts Institute of Technology, Cambridge, Massachusetts 02139, USA
(Received 19 April 2006; published 27 November 2006)

We have generated a new type of biphoton state by cavity-enhanced down-conversion in a type-II phase-matched, periodically poled $KTiOPO_4$ crystal. By introducing a weak intracavity birefringence, we obtained signal and idler photons whose quantum interference was modulated between singlet and triplet signatures according to their arrival-time difference. This cavity-enhanced biphoton source is spectrally bright, yielding a single-mode fiber-coupled coincidence rate of 0.7 pairs/s per mW of pump power per MHz of down-conversion bandwidth.

DOI: 10.1103/PhysRevLett.97.223601 PACS numbers: 42.50.Dv, 03.65.Ud, 03.67.Mn, 42.65.Lm

Spontaneous parametric down-conversion (SPDC) is the principal source for polarization-entangled photon pairs [1], but its ~THz bandwidth makes it ill suited for coupling to the ~MHz bandwidth of an atomic absorption line. What is needed, to make such coupling efficient, is a bright, narrowband source of polarization-entangled photons [2]. Ou and Lu [3] placed a continuous-wave (cw) type-I phase-matched down-converter in an optical cavity that resonated the signal and idler to increase its efficiency and narrow its bandwidth. Wang *et al.* [4] did the same for a pair of cw type-I down-converters, one rotated by 90°, in a ring cavity to produce polarization-entangled photons. We will report the first signal and idler cavity-enhanced operation of a cw type-II down-converter, resulting in a spectrally bright, narrowband source of frequency-degenerate photon pairs. More importantly, by controlling a weak intracavity birefringence, our source generates a new type of biphoton state whose output can be modulated between constructive and destructive quantum interference according to the arrival-time difference between the signal and idler photons.

Consider conventional cw SPDC in a collinear configuration that is type-II phase matched at frequency degeneracy. The biphoton state emerging from the usual timing-compensation crystal is then $|\psi\rangle = (|H,t\rangle|V,t+\tau_p\rangle + e^{i\theta}|V,t\rangle|H,t+\tau_p\rangle)/\sqrt{2}$, in the horizontal-vertical (H-V) basis, where t and $t+\tau_p$ are the times at which the photons would be detected. Ordinarily we have $\theta = 0$, but a half-wave plate can be inserted to make $\theta = \pi$. These two possibilities can be distinguished by the quantum-interference signatures they exhibit when coincidence counting is done in the ±45° basis: $\theta = 0$ ($\theta = \pi$) yields a coincidence dip (peak) that is the signature of a triplet (singlet) state. The situation becomes more complicated—and more interesting—when that down-converter is embedded in a single-ended cavity that resonates the signal and idler. The signal and idler photons resulting from down-conversion of a pump photon may emerge from the output coupler after the same number of round-trips within the cavity, but the times at which these photons leave the cavity may also differ by an integer multiple, $m = 0, \pm1, \pm2, \ldots$, of the cavity round-trip time, τ_c. Thus, the biphoton state associated with a photon pair whose arrival-time difference is $\tau_p + m\tau_c$ is $|\psi, m\rangle = (|H,t\rangle|V,t+\tau_p+m\tau_c\rangle + e^{im\phi}|V,t\rangle|H,t+\tau_p+m\tau_c\rangle)/\sqrt{2}$, where ϕ is the round-trip cavity birefringence, and t and $t+\tau_p+m\tau_c$ are the photon-detection times. Note that $|\tau_p| \sim$ ps whereas $\tau_c \sim$ ns, so that coincidence counting can resolve the round-trip time-bin difference m. By tuning the cavity birefringence to achieve $\phi \neq 0$, we get a new type of biphoton that exhibits time-bin modulated quantum interference in ±45°-basis coincidence counting. Before describing our experimental work, we shall provide a more precise characterization of cavity-enhanced type-II SPDC.

Consider the cw down-conversion configuration shown in Fig. 1. A length-L KTP intracavity compensating crystal (ICC) and a length-L periodically poled $KTiOPO_4$ (PPKTP) crystal are contained inside a single-ended optical cavity, and a length-$L/2$ KTP external compensating crystal (ECC) is employed outside the cavity. The cavity mirrors do not reflect the frequency-ω_P pump, but they do

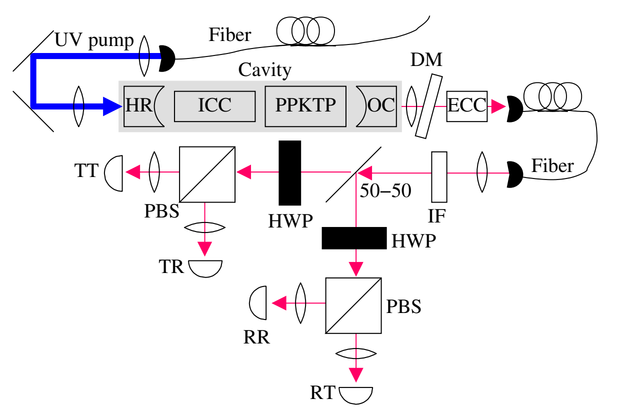

FIG. 1 (color online). Cavity-enhanced SPDC setup. HR, high reflector; ICC, intracavity compensating crystal; ECC, external compensating crystal; OC, output coupler; HWP, half-wave plate; PBS, polarizing beam splitter; DM, dichroic mirror; IF, interference filter; TT, TR, RT, and RR, single-photon detectors.

resonate the frequency-degenerate signal and idler. The pump propagates along the x axes of all three crystals. The y axis of the PPKTP crystal is horizontal, and the y axes of the compensating crystals are vertical. Without the cavity mirrors, ICC has no effect; with the cavity mirrors, ICC provides timing compensation for photons that perform one or more round-trips before exiting the cavity.

Our experiments measured statistics of the time difference, τ, between photon detections made in the H-V or the $\pm 45°$ polarization bases. The H-V coincidence rate is $R_{\rm HV}(\tau) = C|K_{\rm SI}^{(p)}(\tau)|^2$ in terms of the phase-sensitive correlation of the signal and idler, $K_{\rm SI}^{(p)}(\tau)$, and a proportionality constant C, and the $\pm 45°$ rate is $R_{\pm 45}(\tau) = C|K_{\rm SI}^{(p)}(\tau) - K_{\rm SI}^{(p)}(-\tau)|^2/4$. Furthermore, we have [5] $K_{\rm SI}^{(p)}(\tau) \propto \sum_{m=-\infty}^{\infty}\sum_{\ell=0}^{\infty} R^{\ell+|m|/2}e^{im\phi/2}\mathrm{box}_{\tau_0}(\tau - m\tau_c)$, at a signal-idler double resonance, where R is the output coupler's reflectivity and ℓ is the number of common cavity round-trips spent by the signal and idler. Also, $\mathrm{box}_{\tau_0}(\tau) = 1$ for $|\tau| \le \tau_0/2 \equiv |\Delta k'|L/2$ and zero otherwise, which is the time-domain manifestation of the phase-matching function, with $\Delta k'$ being the frequency derivative of the phase mismatch. In our experiment, $\tau_0 \approx 3.5$ ps, $\tau_c \approx 826$ ps, and ϕ was controlled by temperature tuning of the ICC. Setting $R = 0$ reduces $K_{\rm SI}^{(p)}(\tau)$ to the single-pass SPDC result, i.e., the $\ell = m = 0$ term. For $R > 0$, the $m \neq 0$ terms are due to correlations between signal and idler photons that came from the same pump photon but exited the output coupler with the signal photon having taken m more cavity round-trips than the idler did and incurring m times the cavity birefringence. Because the different box functions in $K_{\rm SI}^{(p)}(\tau)$ are nonoverlapping in our experiment, we find that $R_{\rm HV}(\tau) = \sum_{m=-\infty}^{\infty} R_{\rm HV}^{(m)}(\tau)$ and $R_{\pm 45}(\tau) = \sum_{|m|=0}^{\infty} \sin^2(m\phi/2)R_{\rm HV}^{(|m|)}(\tau)$, where $R_{\rm HV}^{(m)}(\tau)$ is the $\mathrm{box}_{\tau_0}(\tau - m\tau_c)$ term in the H-V coincidence rate.

Our experimental setup is shown in Fig. 1. The intracavity compensating crystal was unpoled KTP polished to a length within ± 1 μm of the ~9.7-mm-long PPKTP crystal, as verified by birefringence measurements made with a tunable laser. Each was placed on its own thermoelectric cooler for independent temperature control with 0.01 °C stability. The PPKTP crystal was tuned to frequency degeneracy for SPDC, and the ICC was tuned to control the cavity birefringence. The PPKTP, ICC, and ECC crystals were antireflection coated at 795 nm and 397.5 nm. The ICC and PPKTP were placed inside an optical cavity formed by an input mirror, coated for high reflection at 795 nm and an output coupler that was coated for 92% reflection at 795 nm; both mirrors were also high transmission at 397 nm. The mirrors had 50 mm radii of curvature and were separated by 104.9 mm, which yielded a ~1.21 GHz free spectral range ($\tau_c \approx 826$ ps). The output coupler was mounted on a piezoelectric transducer for cavity-length control.

We used a cw external-cavity diode laser (Toptica) as the pump source, operated near 397.5 nm. The pump light was sent through 2 m of single-mode fiber (StockerYale) that served as a spatial filter, and ~1 mW of power was mode matched into the cavity. Most of the pump light passed through the cavity and was then diverted from the output path by the dichroic mirror (DM). The cavity finesse at 795 nm was measured to be ~55, corresponding to 11% loss per round-trip, which was consistent with the 92% reflectivity of the output coupler and the ~0.3% loss per surface for the crystals. A ~5 mm KTP external compensating crystal was placed outside of the cavity before the aspheric lens that coupled the down-converted light into a single-mode fiber equipped with polarization-control paddles. The resonantly generated down-converted light had a well-defined spatial mode that allowed efficient mode matching into a single-mode fiber (~30%). After the fiber there was a 1 nm interference filter (IF) and a 50-50 beam splitter. The transmitted arm contained a half-wave plate (HWP) set at θ_T and a polarizing beam splitter (PBS) whose transmitted and reflected paths led to single-photon counters TT and TR, respectively. The reflected path from the 50-50 beam splitter contained another HWP (set at θ_R) and a PBS with two detectors (RT and RR) in its output paths. The single-photon detectors were all Perkin-Elmer silicon avalanche photodiodes and their location labels indicate the beam paths (as transmitted T or reflected R) taken at the 50-50 beam splitter and then at the PBS. Weak pump-beam reflections (~17%) at the cavity mirrors created a weak pump modulation as the cavity length was swept.

We measured the coincidence rates between the TT and TR detectors and between the RT and RR detectors. TT and TR detections were also used to provide start and stop signals for collecting arrival-time-difference histograms for comparison with the predicted behavior of $R_{\rm HV}(\tau)$ and $R_{\pm 45}(\tau)$. The RT and RR measurements were always made with $\theta_R = 0$, corresponding to the H-V basis (aligned to the PPKTP's y and z axes). Thus they monitored the maximum coincidence rate to check that the down-conversion remained consistent during data collection. The TT-TR coincidence rate and arrival-time difference histogram were measured either with $\theta_T = 0$ (for the H-V basis) or with $\theta_T = \pi/8$ (for the $\pm 45°$ basis). Data were collected while the cavity length was swept through one free spectral range (FSR) using a 40-s-period triangular waveform. The arrival-time-difference histograms at a signal-idler double resonance, shown in Figs. 2–4, come from 16 minutes of data integration using 38.3 ps time bins. Had the cavity length been locked at a double resonance, the data collection time would have been significantly reduced.

We measured the cavity transmission of a ~795 nm probe beam and tuned the temperature of the ICC to simultaneously resonate both polarizations as the cavity length was swept, after which the probe laser was removed and SPDC coincidence counting was performed. The resulting TT-TR data are shown in Fig. 2, corresponding to the case of zero birefringence, $\phi = 0$. The upper curve is

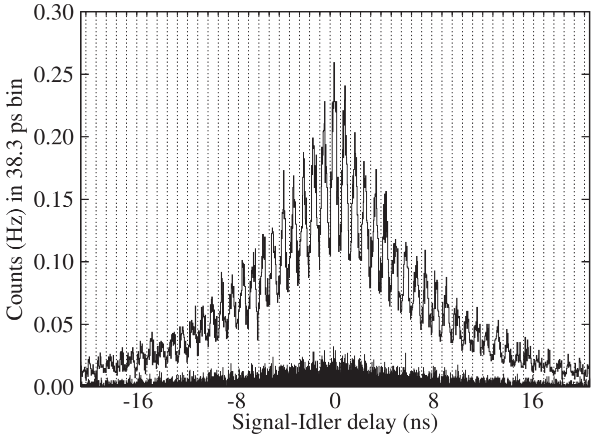

FIG. 2. Arrival-time-difference histograms at zero birefringence, $\phi = 0$, averaged over 16 minutes. Upper curve is for the *H*-*V* basis. The lower filled curve is for the $\pm 45°$ basis.

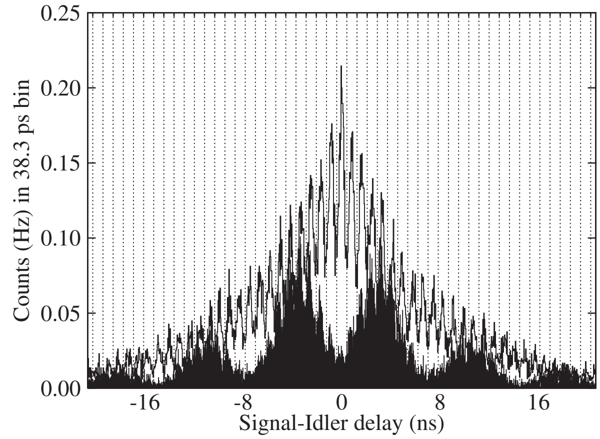

FIG. 3. Similar to Fig. 2 with temperature detuned by 0.53 °C.

the arrival-time-difference histogram for the *H*-*V* basis. Its peaks are separated by the ~826 ps cavity round-trip time τ_c, and broadened—from their 3.5 ps theoretical width—by the 350 ps time jitter of our single-photon counters. Its highest ($\tau = 0$) peak was due to signal-idler pairs that exited the cavity after the same number of round-trips. The filled curve in Fig. 2 is the arrival-time-difference histogram for the $\pm 45°$ basis. The quantum interference was found by taking the ratio of the $\pm 45°$ rate to the *H*-*V* rate. Figure 5 fill *A* shows the ratio of $\pm 45°$-basis coincidences, summed over the peak for each *m* value, to the corresponding sum for *H*-*V*-basis coincidences, after a small background-count correction has been made (0.014 Hz/bin for *H*-*V* and 0.009 Hz/bin for $\pm 45°$). The ratio of the total of the central 41 peaks in the $\pm 45°$ histogram to that for the *H*-*V* histogram was 0.131. This corresponds to a quantum-interference fringe visibility of 76.8%. The >50% visibility is clear evidence of nonclassical behavior. Hence, we expect that a $\phi = 0$ biphoton output from the 50-50 beam splitter in Fig. 1 should be a polarization-entangled triplet [6]. Much of the loss from ideal visibility can be attributed to the reflected pump light, as discussed below. The slight curvature seen in Fig. 5 fill *A* can be attributed to temperature fluctuations of the ICC that were equivalent to an offset of 0.004 °C from the ideal value.

By varying the ICC temperature, while keeping the PPKTP temperature fixed, we were able to control the cavity birefringence precisely. At zero birefringence, the effective lengths of the ICC and PPKTP were the same. By varying the ICC temperature, the effective lengths could be tuned to achieve $\phi = 2\pi T/T_{2\pi}$, where T is the ICC temperature relative to the zero-birefringence temperature, and $T_{2\pi}$ is the temperature shift required to yield $\phi = 2\pi$. Using a 795 nm probe laser, we measured $T_{2\pi} = 4.5$ °C. Thus the $\pm 45°$-basis quantum interference from our cavity-enhanced down-converter should change from a dip (triplet signature), at zero time-bin difference ($m = 0$), to a peak (singlet signature), at $m = T_{2\pi}/2T$.

Data were collected for a series of ICC temperatures, so that the signal and idler resonated at different cavity lengths. Figure 3 shows the results for $T \approx 0.53$ °C, where the upper (filled) curve is the *H*-*V* ($\pm 45°$) histogram. As in Fig. 2, the central ($m = 0$) peak in the *H*-*V* histogram is suppressed in the $\pm 45°$ histogram. For $T \neq 0$, however, the $\pm 45°$ coincidence rate shows the $\sin^2$ oscillation expected from our $R_{\pm 45}(\tau)$ expression, with a period in *m* of 8.90 round-trips (fit to the data). Thus the SPDC output was modulated between states with triplet and singlet signatures, with intermediate behavior occurring at round-trip offsets in between these extremes. Their histogram ratio, shown in Fig. 5 curve *B*, clearly indicates the periodic change from an interference dip (ratio ~0.2) to an interference peak (ratio ~0.8).

The triplet signature recurred whenever the temperature was detuned by a multiple of 4.5 °C. The data for Fig. 4 were taken at $T = 2.26$ °C with $\phi = \pi$. Now, all the even-round-trip peaks are suppressed and all the odd-round-trip peaks are maxima. The ratio alternates between a maxi-

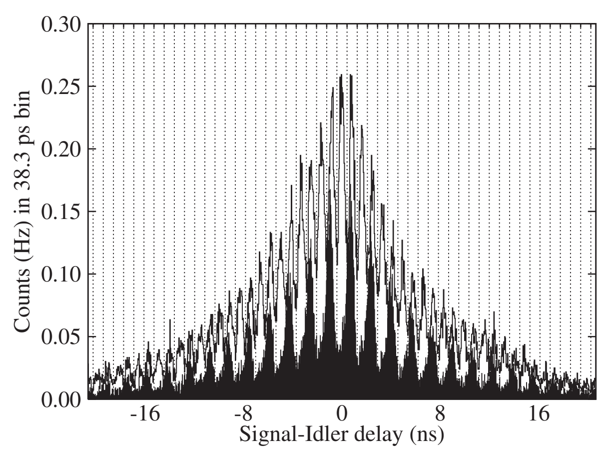

FIG. 4. Similar to Fig. 2 with the temperature detuned by 2.26 °C.

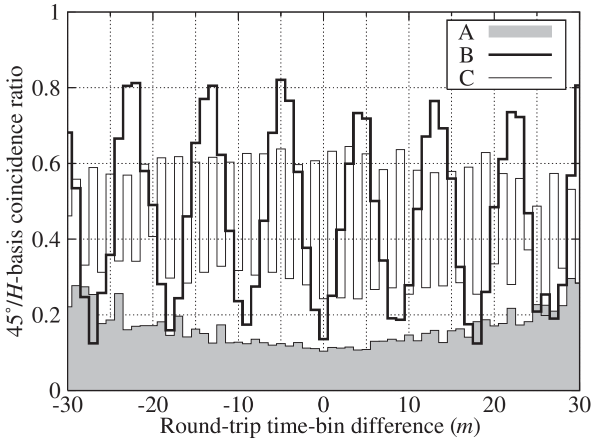

FIG. 5. Ratio of histograms from Figs. 2 (fill A), 3 (curve B), and 4 (curve C) vs round-trip time-bin difference m.

mum and minimum—see Fig. 5 curve C—in agreement with the predicted period of 2 for this temperature detuning. The odd-round-trip quantum-interference peaks are exhibiting polarization singlet behavior. The reduced contrast was partly due to detector time jitter, which causes the counts from one peak to spill into time bins associated with adjacent peaks. This effect also reduced the contrast in Fig. 5 curve B.

The ~17% pump reflection from the output coupler led to down-conversion in the backward pump path in Fig. 1. However, the ECC had the wrong orientation for pairs generated by this backward pump, thus they always produce a ±45°-basis to H-V-basis ratio of 1/2, which reduced our measured quantum-interference visibility. We rotated the ECC by 90°, so that the forward-pump pairs have a 1/2 ratio and the backward pairs exhibit quantum interference. With this arrangement the quantum-interference ratio for the $m = 0$ peak increased from 12%, for the normal-ECC orientation, to 43%, for the rotated-ECC orientation, indicating that 90% of the down-conversion was producing interference either forward or backward. Taking into account the ECC's 5 mm length not being exactly half the length of the 9.7 mm PPKTP crystal, this is expected to be 93.2% for a matched ECC. The depths of the forward and backward dips imply that 18.6% of the pump was reflected, in agreement with the 17% estimate from the transmission measurements. The remaining 6.8% contrast loss comes from unknown sources of signal-idler distinguishability.

The peak TT-TR coincidence rate, during the cavity sweep, for the light collected by the single-mode fiber was 2000 pairs/s per mW of pump power. Because of the 50-50 beam splitter, this is 25% of the pairs from the fiber and 50% of the coincidence rate between the transmitted and reflected sides of the beam splitter. This rate is higher than the 300 pairs/(s mW) obtained from this PPKTP crystal without cavity enhancement and without fiber coupling [6]. From the 280 GHz phase-matching bandwidth, 1.21 GHz FSR, and cavity finesse of 55, the FWHM of the central frequency peaks should be ~22 MHz and should contain about 1/250 of the total output. It follows that our experiment produced 0.7 pairs/s per mW of pump power per MHz of bandwidth at frequency degeneracy. These are pairs from a single fiber-coupled spatial mode, and are post-selected after a 50-50 beam splitter. In contrast, the single-pass source in Ref. [6] produced only 0.001 pairs/(s mW MHz) and the source in Ref. [7] produced 0.014 pairs/(s mW MHz). The type-I cavity-enhanced source in Ref. [4] used a $KbNO_3$ crystal and produced 0.12 pairs/(s mW MHz).

In summary, we have demonstrated cavity-enhanced type-II phase-matched SPDC producing spectrally bright, fiber-coupled biphotons that are suitable for efficient coupling to narrowband atomic absorption lines. We have generated a novel biphoton state that shows time-bin modulated quantum interference that can be controlled by adjusting the cavity birefringence. This unique property may be useful for ultrasensitive detection of weak intracavity birefringence. One may place a normally isotropic material under thermal stress or piezoelectric strain in a zero-birefringence cavity-enhanced biphoton source. Any stress-induced material birefringence would induce a coincidence-rate modulation signature that yields the amount of the material birefringence.

This work was supported by a DoD MURI program under ARO-administered Grant No. DAAD-19-00-1-0177.

*Current address: University of St. Andrews, St. Andrews KY16 9SS, United Kingdom.
Electronic address: chrisk@alum.mit.edu

[1] P. G. Kwiat, K. Mattle, H. Weinfurter, A. Zeilinger, A. V. Sergienko, and Y. Shih, Phys. Rev. Lett. **75**, 4337 (1995); P. G. Kwiat, E. Waks, A. G. White, I. Appelbaum, and P. H. Eberhard, Phys. Rev. A **60**, R773 (1999); F. König, E. J. Mason, F. N. C. Wong, and M. A. Albota, Phys. Rev. A **71**, 033805 (2005); M. Fiorentino, C. E. Kuklewicz, and F. N. C. Wong, Opt. Express **13**, 127 (2005).
[2] J. H. Shapiro and N. C. Wong, J. Opt. B **2**, L1 (2000).
[3] Z. Y. Ou and Y. J. Lu, Phys. Rev. Lett. **83**, 2556 (1999).
[4] H. Wang, T. Horikiri, and T. Kobayashi, Phys. Rev. A **70**, 043804 (2004).
[5] C. E. Kuklewicz, Ph.D. thesis, Massachusetts Institute of Technology, 2005.
[6] C. E. Kuklewicz, M. Fiorentino, G. Messin, F. N. C. Wong, and J. H. Shapiro, Phys. Rev. A **69**, 013807 (2004).
[7] M. Fiorentino, G. Messin, C. E. Kuklewicz, F. N. C. Wong, and J. H. Shapiro, Phys. Rev. A **69**, 041801(R) (2004).